Applied Catalysis B: Environmental 164 (2015) 324–333

Contents lists available at ScienceDirect

Applied Catalysis B: Environmental

journal homepage: www.elsevier.com/locate/apcatb

Pd-MnO_x nanoparticles dispersed on amine-grafted silica: Highly efficient nanocatalyst for hydrogen production from additive-free dehydrogenation of formic acid under mild conditions

Ahmet Bulut[a], Mehmet Yurderi[a], Yasar Karatas[a], Mehmet Zahmakiran[a,*], Hilal Kivrak[b], Mehmet Gulcan[a], Murat Kaya[c]

[a] Department of Chemistry, Yüzüncü Yıl University, 65080 Van, Turkey
[b] Department of Chemical Engineering, Yüzüncü Yıl University, 65080 Van Turkey
[c] Department of Chemical Engineering and Applied Chemistry, Atilim University, 06836 Ankara, Turkey

ARTICLE INFO

Article history:
Received 29 June 2014
Received in revised form 31 August 2014
Accepted 20 September 2014
Available online 28 September 2014

Keywords:
Formic acid
Dehydrogenation
Nanoparticles
Palladium
Manganese oxide

ABSTRACT

Herein we report the development of a new highly active, selective and reusable nanocatalyst for additive-free dehydrogenation of formic acid (HCOOH), which has great potential as a safe and convenient hydrogen carrier for fuel cells, under mild conditions. The new catalyst system consisting of bimetallic Pd-MnO_x nanoparticles supported on aminopropyl functionalized silica (Pd-MnO_x/SiO_2-NH_2) was simply and reproducibly prepared by deposition–reduction technique in water at room temperature. The characterization of Pd-MnO_x/SiO_2-NH_2 catalyst was done by the combination of multipronged techniques, which reveals that the existence of highly crystalline individually nucleated Pd(0) and MnO_x nanoparticles (d_{mean} = 4.6 ± 1.2 nm) on the surface of aminopropyl functionalized silica. These supported Pd-MnO_x nanoparticles can catalyze the additive-free dehydrogenation of formic acid with record activity (TOF = 1300 h^{-1}) at high selectivity (>99%) and conversion (>99%) under mild conditions (at 50 °C and under air). Moreover, easy recovery plus high durability of these supported Pd-MnO_x nanoparticles make them a reusable heterogeneous catalyst in the additive-free dehydrogenation of formic acid.

1. Introduction

Hydrogen is a globally accepted clean energy carrier, which could solve the world energy problem and reduce the environmental pollution originated from the fossil fuels [1,2] as the hydrogen can be act as an environmentally friendly energy vector to end users when combined with proton exchange membrane (PEM) fuel cells [3,4]. However, controlled storage and release of hydrogen are still technological barriers in the fuel cell based hydrogen economy [1–4]. Among the various kinds of hydrogen storage materials [1–6], formic acid (FA, HCOOH), a major product formed in biomass processing, has attracted more attention as a suitable hydrogen storage material due to its high energy density, stability and non-toxicity [7]. FA can catalytically be decomposed via dehydrogenation ($HCOOH \rightarrow H_2 + CO_2$) and dehydration ($HCOOH \rightarrow H_2O + CO$) pathways [8]. The latter is the unwanted reaction and should be circumvented for the subsequent conversion of hydrogen into electrical energy in the fuel cells, as it produces CO impurity, which is toxic to fuel cell catalysts [9].

Recently, many efforts in the development of homogeneous catalysts for the selective dehydrogenation of FA have been made [10]. Although, some of these homogeneous catalysts provide high activities and selectivities in FA dehydrogenation, their difficult separation from the reaction mixture and requirement of ligands/additives hinder their practical applications. At this concern, because of the advantages of nanocatalysis [11], the current research has been concentrated on the development of metal nanoparticles (NPs) possessing high activity and selectivity in the dehydrogenation of FA [7]. Monometallic Pd, Au and Pt based-NPs can catalyze the dehydrogenation of FA only when they used with some additives (sodium formate, triethylamine, etc.) [12–15]. However, multi-metallic NPs such as AuPd [16], AgPd [17], PdNi [18], PdNi@Ni [18], Au@Pd [19], Ag/Pd [20], and CoAuPd [21] provide notable activities in the dehydrogenation of FA in the absence of any additives at low temperatures. As a common feature, all of these

* Corresponding author. Fax: +90 432 225 18 06.
E-mail address: zmehmet@yyu.edu.tr (M. Zahmakiran).

http://dx.doi.org/10.1016/j.apcatb.2014.09.041
0926-3373/

multi-metallic NPs systems involve Pd metal, which is highly active metal in FA dehydrogenation like Au and Pt. However, monometallic Pd is inclined to deactivation due to adsorption of poisonous carbon monoxide (CO), which can be formed as intermediate during the dehydrogenation of FA in the absence of promoters such as sodium formate [7,8]. At this concern, incorporation of another metal that has better CO resistance than Pd, seems to be a promising solution to avoid CO-deactivation of Pd active sites [16–21]. Therefore, it is highly inviting to further increase catalytic performance and CO tolerance of Pd NPs, and lower the cost of nanocatalyst by integration of low-cost metals.

Aside from the tuning catalyst composition, the design and/or selection of support material for the ligand-free Pd NPs is also another key factor for the improvement of the catalytic performance of Pd NPs in FA dehydrogenation. More recently, Yamashita et al. [22] reported that Pd NPs supported on $-N(CH_3)_2$ bearing resin provide better activity than that of supported on neat resin in FA dehydrogenation. They explained that the existence of surface bound $-N(CH_3)_2$ group facilitates the dissociation of O–H bond in formic acid and enhances dehydrogenation rate.

Herein, we report the preparation and characterization of a new Pd-based bimetallic nanocatalyst, Pd-MnO_x NPs supported on 3-aminopropyl functionalized silica (SiO_2-NH_2), hereafter referred to as Pd-MnO_x/SiO_2-NH_2, plus their excellent catalytic performance in terms of activity, selectivity and reusability in the additive-free dehydrogenation of FA at low temperatures (<70 °C). Pd-MnO_x/SiO_2-NH_2 can simply and reproducibly be prepared through the conventional impregnation followed by subsequent sodium borohydride ($NaBH_4$) reduction in water at room temperature. The characterization of Pd-MnO_x/SiO_2-NH_2 was performed by using advanced analytical techniques including inductively coupled plasma-optical emission spectroscopy (ICP-OES), powder X-ray diffraction (PXRD), X-ray photoelectron spectroscopy (XPS), conventional transmission electron microscopy (CTEM), high resolution transmission electron microscopy (HRTEM), scanning transmission electron microscopy (STEM), scanning transmission electron microscope-energy dispersive X-ray spectroscopy (STEM-EDX), high angle annular dark field-scanning transmission electron microscopy (HAADF-STEM) and CO-stripping voltammetry. The sum of their results shows that the formation of separately nucleated Pd(0) and MnO_x NPs with an average size of 4.6 ± 1.2 nm on the surface of aminopropyl functionalized silica. The resulting Pd-MnO_x/SiO_2-NH_2 catalyst is acting as highly selective (>99%) heterogeneous catalyst in the additive-free dehydrogenation of FA with the unprecedented catalytic activity (TOF = 1300 h^{-1} at 50 °C) at complete conversion (>99%). Moreover, the exceptional durability of Pd-MnO_x NPs against to agglomeration, leaching and CO poisoning makes them reusable catalytic material in the additive-free dehydrogenation of FA.

2. Experimental

2.1. Materials

Palladium(II) nitrate dihydrate ($Pd(NO_3)_2{\cdot}2H_2O$) (~40% Pd basis), silica gel (40–63 μm), aminopropyltriethoxysilane ($H_2N(CH_2)_3Si(OC_2H_5)_3$), sodium borohydride ($NaBH_4$), ninhydrin ($C_9H_6O_4$), toluene ($C_7H_8$) and sodium hydroxide (NaOH) were purchased from Sigma-Aldrich®, manganese (II) dichloride dihydrate ($MnCl_2{\cdot}2H_2O$), formic acid (CH_2O_2) were purchased from Merck® and all them were used without further purification. Deionized water was distilled by water purification system (Milli-Q Water Purification System). All glassware and Teflon-coated magnetic stir bars were washed with acetone and copiously rinsed with distilled water before drying in an oven at 150 °C.

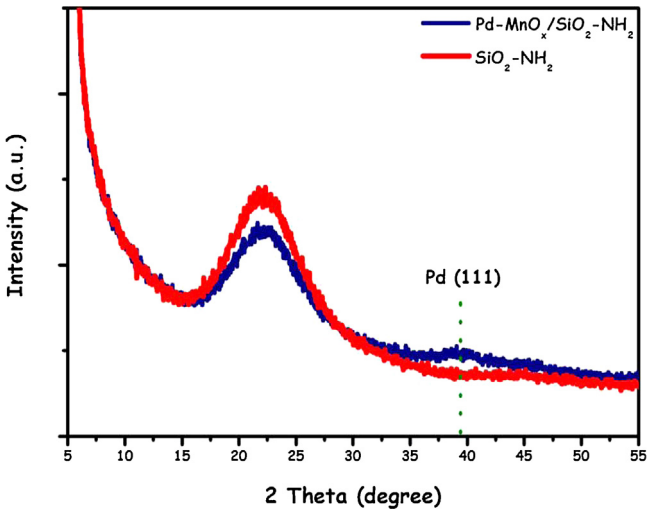

Fig. 1. P-XRD patterns of SiO_2-NH_2 and Pd-MnO_x/SiO_2-NH_2.

2.2. Characterization

Pd and Mn contents of the samples were determined by ICP-OES (Leeman, Direct Reading Echelle) after each sample was completely dissolved in a mixture of HNO_3/HCl (1/3 ratio). Powder X-ray diffraction (XRD) patterns were recorded with a MAC Science MXP 3TZ diffractometer using Cu Kα radiation (wavelength 1.54 Å, 40 kV, 55 mA). CTEM, HRTEM, STEM, and HAADF-STEM samples were prepared by dropping one drop of dilute suspension on copper coated carbon TEM grid and the solvent was then dried. The conventional TEM was carried out on a JEOL JEM-200CX transmission electron microscopes operating at 120 kV. HRTEM, STEM, and HAADF-STEM were run on a JEOL JEM-2010F transmission electron microscope operating at 200 kV. Oxford EDXS system and Inca software were used to collect and process STEM-EDX data. The XPS analyses were performed on a Physical Electronics 5800 spectrometer equipped with a hemispherical analyzer and using monochromatic Al Kα radiation (1486.6 eV, the X-ray tube working at 15 kV and 350 W, and pass energy of 23.5 eV). The gas generated from the decomposition of formic acid was analyzed by FID-2014 and TCD-2014 GC analyzers (Shimadzu). CV measurements were carried out in a conventional three-electrode cell with Pt wire as a counter electrode and Ag/AgCl as a reference electrode with a CHI 660E potentiostat.

2.3. Preparation of amine functionalized silica (SiO_2-NH_2)

The functionalization of the silica was carried out by adding a desired amount of APTS to 30 mL of dry toluene containing 500 mg of silica. The resulting slurry was allowed to stir for 12 h. The white solid was filtered and washed repeatedly with toluene. The white amine-functionalized silica (SiO_2-NH_2) was dried in a vacuum oven (100 °C and 10^{-1} Torr) and used for further application. The presence of $-NH_2$ groups on SiO_2 was shown by high resolution XPS spectrum of SiO_2-NH_2 (Fig. S-1) and quantified by the colorimetric ninhydrin method [23].

2.4. Preparation of Pd/SiO_2-NH_2, MnO_x/SiO_2-NH_2 and Pd-MnO_x/SiO_2-NH_2 (Pd:Mn = 0.6:0.4) catalysts

In a three separate experiments, 5.0 mL aqueous solutions of (a) Pd-MnO_x/SiO_2-NH_2: 7.6 mg $Pd(NO_3)_2{\cdot}2H_2O$ (29 μmol Pd), 3.1 mg $MnCl_2{\cdot}2H_2O$ (19 μmol Mn) and 100 mg SiO_2-NH_2 (100 μmol NH_2); (b) Pd/SiO_2-NH_2: 11.8 mg $Pd(NO_3){\cdot}2H_2O$ (45 μmol Pd) and 100 mg SiO_2-NH_2 (100 μmol NH_2); (c) MnO_x/SiO_2-NH_2: 7.3 mg

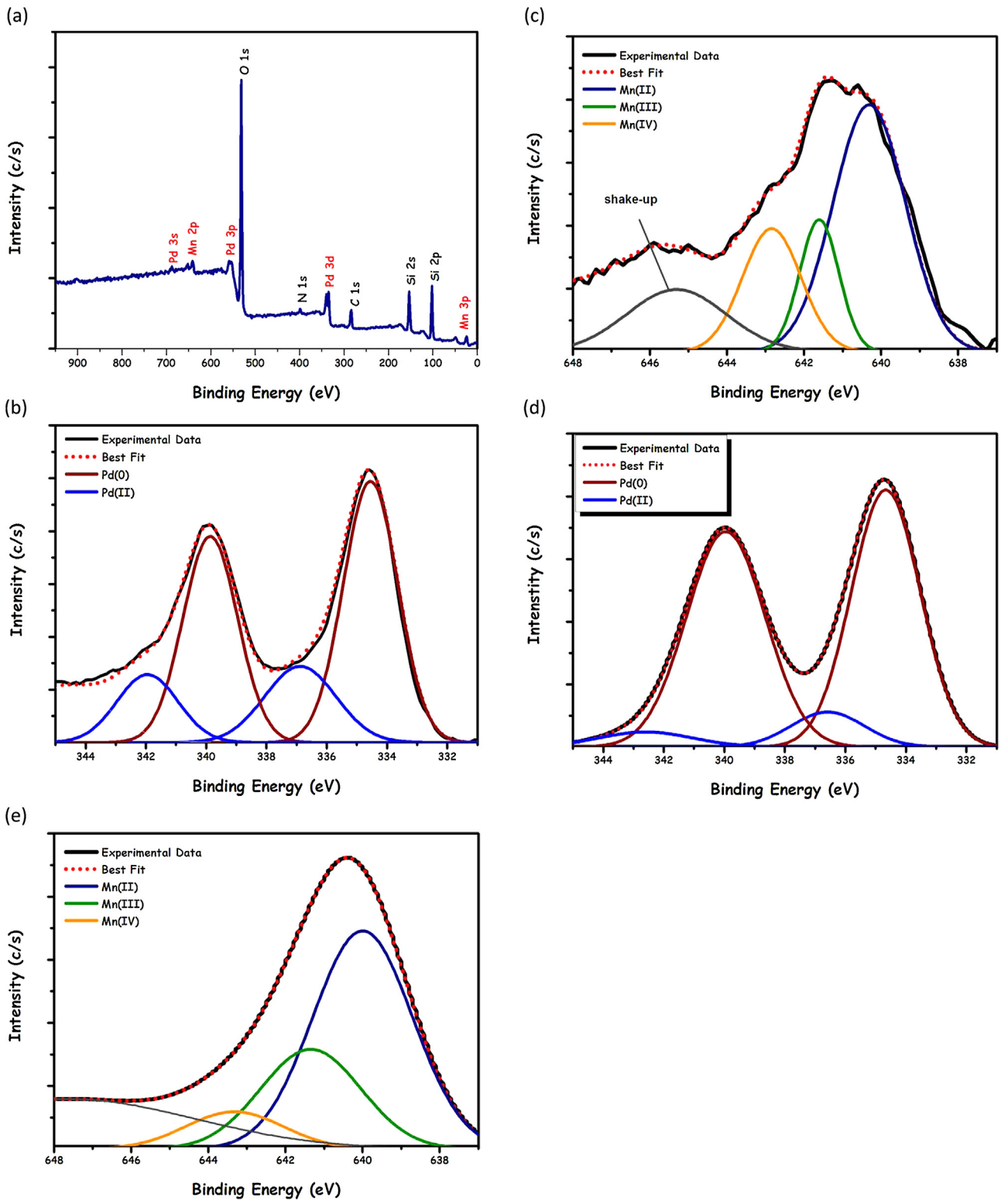

Fig. 2. (a) A survey XPS spectrum of Pd-MnO_x/SiO_2-NH_2, (b) high resolution Pd 3d XPS spectrum of Pd-MnO_x/SiO_2-NH_2, (c) high resolution Mn 2p XPS spectrum of Pd-MnO_x/SiO_2-NH_2, (d) high resolution Pd 3d XPS spectrum of Pd-MnO_x/SiO_2-NH_2 after 5 min of Ar etching, (e) high resolution Mn 2p XPS spectrum of Pd-MnO_x/SiO_2-NH_2 after 5 min of Ar etching.

$MnCl_2{\cdot}2H_2O$ (45 μmol Mn) and 100 mg SiO_2-NH_2 (100 μmol NH_2) are mixed. Then, fresh 1.0 mL $NaBH_4$ (32 mg, 0.8 mmol) solution in water was added separately to these mixtures and the resulting solutions were stirred for half an hour under air at room temperature. After centrifugation (6000 rpm, 5 min), copious washing with water (3 × 20 mL), filtration, and drying in oven at 100 °C, Pd/SiO_2-NH_2, MnO_x/SiO_2-NH_2 and Pd-MnO_x/SiO_2-NH_2 catalysts were obtained as powders.

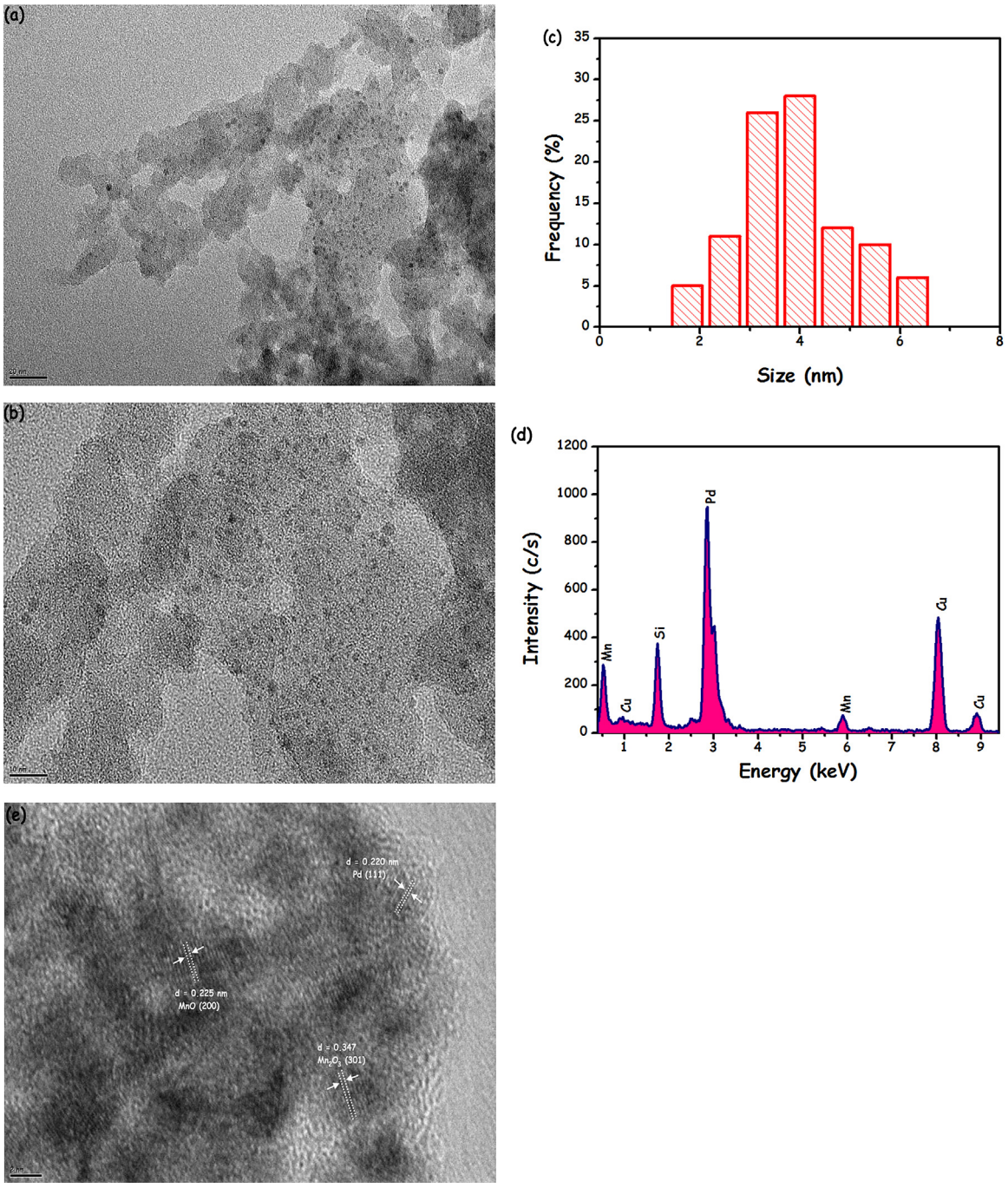

Fig. 3. (a–c) CTEM images of Pd-MnO_x/SiO_2-NH_2 in different magnifications, (d) the size histogram of Pd-MnO_x/SiO_2-NH_2, (e) STEM-EDX spectrum of Pd-MnO_x/SiO_2-NH_2 collected from the region given in (a), (f) HRTEM image of Pd-MnO_x/SiO_2-NH_2.

2.5. Determination of the catalytic activity of Pd-MnO_x/SiO_2-NH_2 catalyst in the additive-free dehydrogenation of formic acid

The catalytic activity of Pd-MnO_x/SiO_2-NH_2 in the dehydrogenation of FA was determined by measuring the rate of hydrogen generation. The volume of released gas during the reaction was monitored using the gas burette by water displacement. Before starting the catalytic activity test, a jacketed one necked reaction flask (50.0 mL) containing a Teflon-coated stir bar was placed on a magnetic stirrer (Heidolph MR-3004) and thermostated to $60.0 \pm 0.1\,^{\circ}C$ by circulating water through its jacket from a constant temperature bath (Lab Companion RW-0525). In a typical experiment, Pd-MnO_x/SiO_2-NH_2 catalyst was weighed and transferred into the reaction flask, and then 9.0 mL H_2O was added into the reaction flask and this mixture was stirred for 15 min to achieve thermal equilibrium. Next, 0.5 mL aqueous FA solution (0.1 mL FA + 0.4 mL H_2O) was added into the reaction flask via its septum by using a 1.0 mL gastight syringe and the catalytic reaction was started ($t = 0$ min) by stirring the mixture at 600 rpm.

2.6. NaOH trap experiment

To determine CO_2 to H_2 molar ratio in the gas mixture generated during the Pd-MnO_x/SiO_2-NH_2 catalyzed dehydrogenation of aqueous FA solution (10 mL of 265 mM), NaOH trap experiment was performed as reported elsewhere [14–17]. In this experiment,

the trap (10 M NaOH solution) was placed between the jacketed reactor and gas burette. The generated gas during the reaction was passed through the NaOH trap and the CO_2 was captured. Next, the volume of the gas generated from the dehydrogenation of FA was monitored and compared to those without trap experiment.

2.7. Isolability and reusability of Pd-MnO_x/SiO_2-NH_2 catalyst in the additive-free dehydrogenation of formic acid

After the first run of catalytic dehydrogenation of aqueous FA solution starting with Pd-MnO_x/SiO_2-NH_2 at 60 ± 0.1 °C, the catalyst was isolated from reaction solution by centrifugation and washed with excess water, then dried at 100 °C. The dried catalyst was weighted and used again in the catalytic dehydrogenation of aqueous FA solution (10 mL of 265 mM) at 60 ± 0.1 °C.

2.8. CO-stripping voltammetry measurements

5 mg catalyst was dispersed in 1.0 mL Aldrich 5% Nafion® solution to obtain the catalyst ink. Next, 5.0 μL of the ink was spread on the surface of the glassy carbon electrode. All electrolyte solutions were deaerated with high-purity nitrogen for at least 30 min prior to any measurement. For CO stripping voltammetry, the 0.5 M H_2SO_4 solution was first bubbled with pure nitrogen for 30 min in order to remove the dissolved oxygen. CO was then purged into solution for 20 min to allow complete adsorption of CO onto the electrocatalyst, while maintaining a constant potential at 0.0 V. Excess CO was then purged with nitrogen for 30 min.

3. Results and discussion

3.1. Preparation and characterization of bimetallic Pd-MnO_x nanoparticles supported on amine-grafted silica (Pd-MnO_x/SiO_2-NH_2)

Bimetallic Pd-MnO_x NPs supported on 3-aminopropyl functionalized silica (Pd-MnO_x/SiO_2-NH_2) were simply and reproducibly prepared by following the procedure comprising of the conventional impregnation of Pd^{2+} and Mn^{2+} onto support and their subsequent $NaBH_4$ reduction in water all at room temperature. After centrifugation, copious washing with water, and drying, Pd-MnO_x/SiO_2-NH_2 catalyst was obtained as black powders and characterized by ICP-OES, P-XRD, XPS, TEM, HRTEM, STEM, STEM-EDX, and HAADF-STEM. The elemental composition of the as-prepared catalyst was found to be $Pd_{0.62}Mn_{0.38}$/SiO_2-NH_2 (1.82 wt% Pd and 0.6 wt% Mn loadings correspond to 17.4 μmol Pd and 10.9 μmol Mn and 1 mmol NH_2/g SiO_2) by ICP-OES analyses and ninhydrin method [23]. P-XRD patterns of Pd-MnO_x/SiO_2-NH_2 and SiO_2-NH_2 are given in Fig. 1. Pd-MnO_x/SiO_2-NH_2 shows only the diffraction line of Pd (1 1 1) plane at 39.1° [16], very weak intensity of this Bragg peak and the absence of other diffraction lines for Pd and Mn might be attributed to their both small size (*vide infra*) and low loadings (<5 wt%) to support material.

XPS measurements were performed to investigate both the composition and the chemical state of the catalyst. Fig. 2(a) shows the XPS survey spectrum that reveals the existence of Si, N, C, Mn, Pd and O elements in the sample. The high resolution Pd 3d and Mn 2p XPS spectra (Fig. 2(b) and (c)) and their deconvulation reveal that the chemical states of Pd and Mn in the catalyst are Pd^0 (Pd $3d_{5/2}$ 334.6 eV; Pd $3d_{3/2}$ 339.8 eV), Pd^{2+} (Pd $3d_{5/2}$ 336.9 eV; Pd $3d_{3/2}$ 342 eV) [24] and those of Mn are Mn^{2+} (Mn $2p_{3/2}$ 640.3 eV), Mn^{3+} (Mn $2p_{3/2}$ 641.6 eV), Mn^{4+} (Mn $2p_{3/2}$ 642.8 eV) [25,26] and the shake-up peak originates from the charge transfer from the outer electron shell to an unoccupied orbit with higher energy during photoelectron process [26]. After Ar sputtering for only 5 min, most of the oxide states of Pd (PdO) were removed and Pd^0 became the main state (Fig. 2(d)). However, mixed oxide forms of Mn (MnO_x) protect their assets in the sample, in which Mn^{2+} and Mn^{3+} are dominant species, despite of Ar etching (Fig. 2(e)). Actually, it is not unexpected result, as the high oxophilicty of Mn makes Mn^0 NPs highly reactive when exposed to air and leads to formation of mixed Mn oxide forms with high stability under aerobic conditions [27,28].

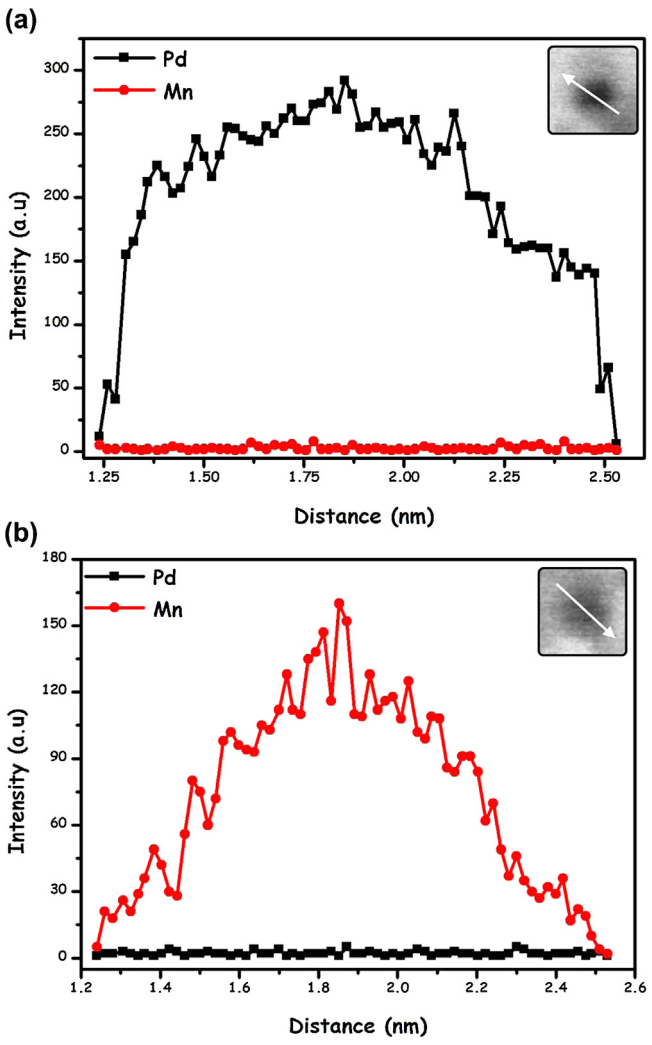

Fig. 4. The distribution of components in the Pd-MnO_x NPs obtained by the line-scan analyses using STEM-EDX along the white arrow on the HAADF-STEM images of Pd-MnO_x/SiO_2-NH_2 given in the insets of (a) and (b).

CTEM, HRTEM, and STEM-EDX analyses were done to investigate the size, morphology and composition of Pd-MnO_x/SiO_2-NH_2 catalyst. CTEM images of Pd-MnO_x/SiO_2-NH_2 are given in Fig. 3(a and b), which reveal that the presence of well-dispersed Pd-MnO_x nanoparticles. The mean particle size of the physical mixture of Pd and MnO_x NPs was found to be 4.6 ± 1.2 nm from CTEM images by using NIH image program [29], whereby >100 non-touching particles were counted, and the corresponding size histogram is given in Fig. 3(c). EDX analysis (Fig. 3(d)) during the STEM observation of Pd-MnO_x/SiO_2-NH_2 from many different areas confirmed the presence of Pd and Mn in the analyzed regions. HRTEM image of Pd-MnO_x/SiO_2-NH_2 given in Fig. 3(e) reveals the highly crystalline nature of Pd-MnO_x NPs and the lattice spacing distances of three individual spherical NPs were measured to be 0.220, 0.225, and 0.357 nm, which corresponds to Pd (1 1 1) [16], MnO (2 0 0) [30], and Mn_2O_3 (3 0 1) [31] crystalline fringes, respectively.

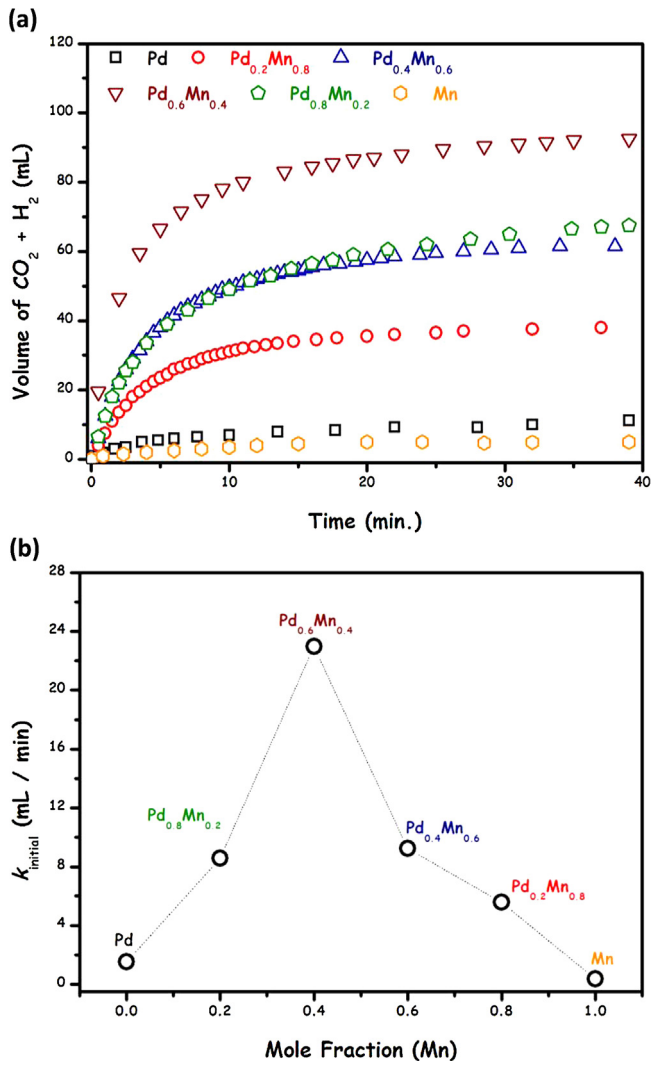

Fig. 5. The plots of (a) the volume of the generated gas ($CO_2 + H_2$) versus time at different Pd and Mn mole fractions, (b) rate of gas generation versus Mn mole fractions for Pd-MnO_x/SiO_2-NH_2 catalyzed dehydrogenation of FA at 60.0 ± 0.1 °C.

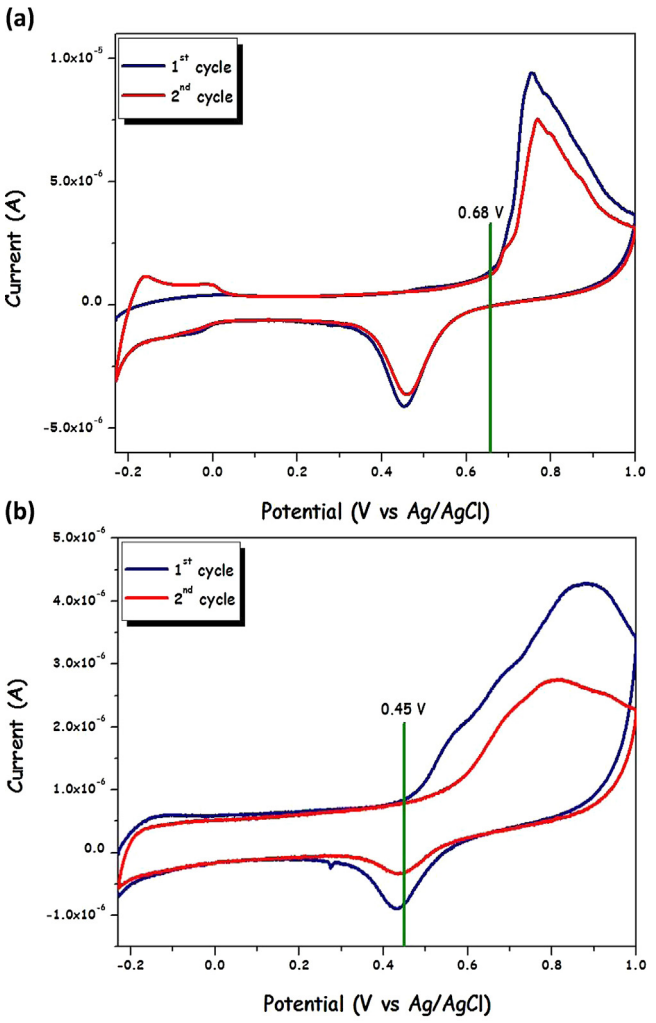

Fig. 6. CO-stripping voltammograms for (a) Pd/SiO_2-NH_2 and Pd-MnO_x/SiO_2-NH_2 catalysts in H_2SO_4 solution at 10 mV s^{-1} scan rate.

The compositional analysis of Pd-MnO_x/SiO_2-NH_2 was also done by HAADF-STEM. Fig. 4 shows the representative results of these HAADF-STEM-line analyses. STEM images of Pd-MnO_x NPs given in the inset of Fig. 4(a) and (b) do not show any darker and brighter regions observed for core/shell structures [32–34]. Moreover, when the distribution of the elements in the randomly chosen Pd-MnO_x NPs was assessed by using the line scanning analysis in the STEM-EDX mode, we cannot see the overlap of Pd and Mn signals that can be assignable to the formation of alloy structure for Pd-MnO_x NPs. The sum of the results gained from HRTEM and HAADF-STEM analyses reveals that the separate nucleation of Pd(0) and MnO_x NPs takes place on SiO_2-NH_2 support in our followed synthesis protocol.

3.2. *Effect of separately nucleated MnO_x on the activity of Pd nanoparticles in the additive-free dehydrogenation of formic acid*

In a series of experiments, the catalytic activities of Pd-MnO_x/SiO_2-NH_2 catalysts (in all [catalyst] = 2.1 mM) with various Pd:Mn molar ratios were tested in the dehydrogenation of FA at 60 °C in the absence of additives (Fig. 5(a)). Fig. 5(b) shows the variation in the catalytic activity of Pd-MnO_x/SiO_2-NH_2 in terms of gas generation rates with Mn mole fractions. The activity increases with increasing Mn mole ratio up to 0.4 and then decreases. The

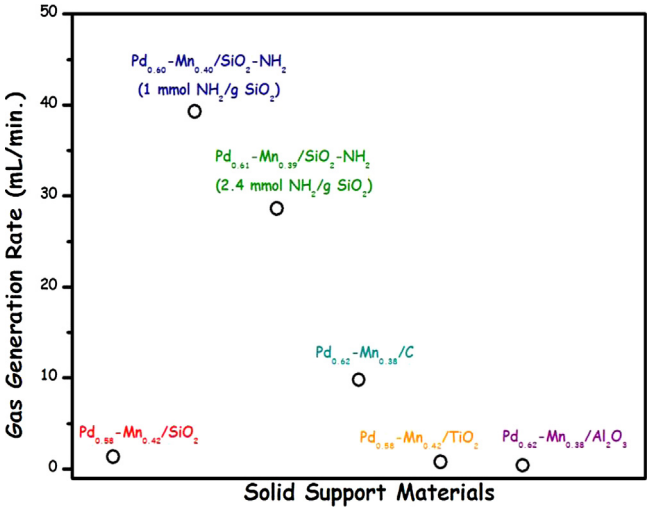

Fig. 7. Gas generation rate (mL/min) versus support materials for the additive-free dehydrogenation of FA catalyzed by $Pd_{0.58}$-$Mn_{0.42}$/SiO_2, $Pd_{0.60}$-$Mn_{0.40}$/SiO_2-NH_2 (1.0 mmol NH_2/g SiO_2), $Pd_{0.61}$-$Mn_{0.39}$/SiO_2-NH_2 (2.4 mmol NH_2/g SiO_2), $Pd_{0.57}$-$Mn_{0.43}$/Al_2O_3, $Pd_{0.58}$-$Mn_{0.42}$/TiO_2 and $Pd_{0.62}$-$Mn_{0.38}$/C catalysts.

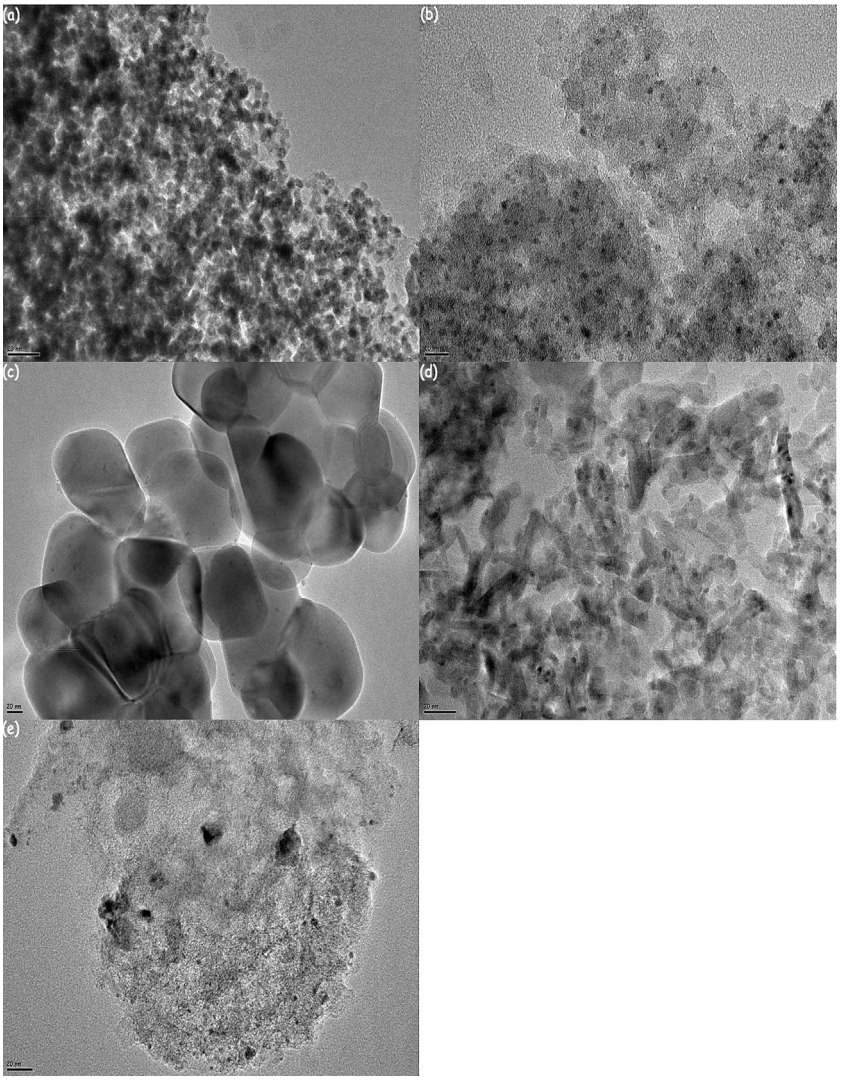

Fig. 8. CTEM images of (a) $Pd_{0.58}$-$Mn_{0.42}/SiO_2$ (b) $Pd_{0.61}$-$Mn_{0.39}/SiO_2$-NH_2 (2.4 mmol NH_2/g SiO_2), (c) $Pd_{0.58}$-$Mn_{0.42}/TiO_2$, (d) $Pd_{0.57}$-$Mn_{0.43}/Al_2O_3$, (e) $Pd_{0.62}$-$Mn_{0.38}$/C catalysts.

observation of cone shaped activity of Pd-MnO_x/SiO_2-NH_2 catalyst is indicating that neither Pd nor Mn has enough activity to catalyze dehydrogenation of FA and $Pd_{0.6}Mn_{0.4}$ is the optimum catalyst for the dehydrogenation of FA. It was further supported by the result of a control experiment in which the physical mixture of Pd/SiO_2-NH_2 and Mn/SiO_2-NH_2 (in Pd:Mn molar ratio of 0.57:0.43) exhibits lower activity than that of $Pd_{0.6}Mn_{0.4}/SiO_2$-NH_2 catalyst for FA dehydrogenation under identical conditions (Fig. S-2). In all of these aforementioned experiments, the generated gas over Pd-MnO_x/SiO_2-NH_2 catalyzed dehydrogenation of FA was identified by gas chromatography (GC) and NaOH trap experiments (Fig. S-3) [14,35], since FA dehydrogenation is generally associated with the dehydration at relatively high reaction temperatures (>60 °C) [7]. Their results revealed that the generated gas is H_2 and CO_2 with the H_2:CO_2 molar ratio of 1.0:1.0 and no CO was detected (DL for CO ~ 10 ppm). This indicates that CO-free H_2 generation can be achieved from aqueous FA solution by Pd-MnO_x/SiO_2-NH_2, which is very important for fuel cell applications [9].

In order to shed some light on the effect of MnO_x NPs on the activity of Pd NPs, we conducted CO-stripping voltammetry measurements on Pd/SiO_2-NH_2 and Pd-MnO_x/SiO_2-NH_2 catalysts. Fig. 6(a) and (b) gives CO-stripping voltammograms for Pd/SiO_2-NH_2 and Pd-MnO_x/SiO_2-NH_2 catalysts. Firstly, the onset potential for CO oxidation on Pd-MnO_x/SiO_2-NH_2 (0.45 V) was found to be lower than that on Pd/SiO_2-NH_2 (0.68 V). In addition, CO oxidation peak current decreased severely after the first scan for Pd-MnO_x/SiO_2-NH_2 catalyst, which is indicative of weaker CO absorption on Pd-MnO_x/SiO_2-NH_2 than that of on Pd/SiO_2-NH_2. These two findings clearly reveal that CO poisoning resistance of Pd NPs is significantly enhanced by the existence of separately nucleated MnO_x NPs, which acts as CO-sponge around the catalytically active Pd NPs. It explains the higher activity of Pd-MnO_x/SiO_2-NH_2 catalyst with respect to Pd/SiO_2-NH_2 in the FA dehydrogenation. In parallel to our findings, El-Deab et al. showed that the electrocatalytic activity of Pt towards the oxidation of formic acid is significantly enhanced upon the electrodeposition of MnO_2 [36].

3.3. *Effect of surface-grafted amine on the activity of Pd-MnO_x NPS in the additive-free dehydrogenation of formic acid*

In order to understand the effect of surface-grafted amine group on the catalytic reactivity of Pd-MnO_x NPs, we compared the catalytic activity of Pd-MnO_x NPs, which were supported on SiO_2 that functionalized with various amounts of amine group (0.0, 1.0 and 2.4 mmol NH_2/g SiO_2), in the additive-free dehydrogenation of FA under the same conditions (10 mL 265 mM FA at 60 °C). The activity order depending on the amine loading was found to be 1.0 mmol NH_2/g SiO_2 (39.3 mL/min for

$Pd_{0.60}$-$Mn_{0.40}$ NPs) > 2.4 mmol NH_2/g SiO_2 (28.6 mL/min for $Pd_{0.61}$-$Mn_{0.39}$ NPs) > amine-free SiO_2 (1.35 mL/min for $Pd_{0.58}$-$Mn_{0.42}$ NPs) (Fig. 7). The higher reactivity of Pd-MnO_x NPs supported on amine-grafted silica supports can be explained by the existence of $-NH_2$ group on the surface. According to the established mechanism of amine assisted metal catalyzed dehydrogenation of FA [13,22], O–H bond cleavage is facilitated with the assistance of $-NR_2$ group as a proton scavenger and leads to the formation of metal–formate species along with a $-[NR_2H]^+$ group. Then, metal–formate complex undergo further dehydrogenation with $-[NR_2H]^+$ species to produce molecular hydrogen and CO_2 via β-elimination pathway. Therefore, it is reasonable to understand that the existence of surface-grafted amine in our support can provide a basic environment around Pd-MnO_x NPs, which benefits the O–H bond dissociation that is subsequently associated with the C–H bond cleavage from the metal–formate intermediate to release H_2 [13,22]. More recently, this strong interaction between metal nanoparticles and amine group grafted on silica support in the catalytic formic acid dehydrogenation has been named as "Strong Metal-Molecular Support Interaction" (SMMSI) by Xu and co-workers [37].

On the other hand, the observed activity drop at 2.4 mmol NH_2/g SiO_2 loading can be explained by taking two factors into consideration: the size of Pd-MnO_x NPs and their surface coverage by $-NH_2$ group of APTS. CTEM images given in Fig. 8(a) and (b) shows that Pd-MnO_x NPs size decreases from 7.4 ± 1.9 to 2.9 ± 0.9 nm by the increase of amine concentration from 0.0 to 2.4 mmol NH_2/g SiO_2. We may thus expect that the surface area and further the catalytic activity of NPs, first increase with increasing amine concentration. However, as the surface-grafted amine concentration increases, NPs surface is more covered by the amine group causing a decrease in the catalytic activity [38,39].

The uniqueness of Pd-MnO_x NPs and SiO_2-NH_2 support combination was also compared with the most commonly used solid support materials (Al_2O_3, TiO_2 and C). The catalytic activities of $Pd_{0.57}$-$Mn_{0.43}$/Al_2O_3, $Pd_{0.58}$-$Mn_{0.42}$/TiO_2 and $Pd_{0.62}$-$Mn_{0.38}$/C catalysts prepared by the same method were investigated in the additive-free dehydrogenation of FA under identical conditions (10 mL 265 mM FA at 60 °C). The results of these experiments revealed that the best catalytic performance in terms of gas generation rate (mL/min) can be achieved by $Pd_{0.6}$-$Mn_{0.4}$/SiO_2-NH_2 catalyst (Fig. 7). CTEM analyses conducted on these catalytic materials (Fig. 8(c)–(e)) showed that the formation of large size Pd-MnO_x NPs on the surface of these solid supports.

3.4. Initial kinetic studies for Pd-MnO_x/SiO_2-NH_2 catalyzed additive-free dehydrogenation of formic acid

The effects of catalyst concentration and temperature on the rate of Pd-MnO_x/SiO_2-NH_2 catalyzed additive-free dehydrogenation of FA were studied. Fig. 9(a) shows the plot of the volume of generated gas ($CO_2 + H_2$) versus the reaction time for the additive-free dehydrogenation of FA at 60 °C and different catalyst concentrations. It should be noted that, the complete conversion of FA is achieved by using 1.4 mol% catalyst (corresponds to only 0.8 mol% Pd) within 11 min. The reaction rates for each catalyst concentration were calculated from the linear portion of each plot comprising reaction duration of 11 min. The logarithmic plot of the reaction rates versus catalyst concentrations gives the line with a slope of 1.16 (Fig. 9(b)), which indicates that the reaction is close to first-order with respect to the catalyst concentration. Fig. 10(a) gives the graph of the volume of generated gas ($CO_2 + H_2$) versus the reaction time for Pd-MnO_x/SiO_2-NH_2 catalyzed dehydrogenation of FA ([catalyst] = 2.80 mM and [FA] = 265 mM) at different temperatures. Pd-MnO_x/SiO_2-NH_2 catalyst can catalyze the additive-free dehydrogenation of FA at temperature as low as 20 °C with an

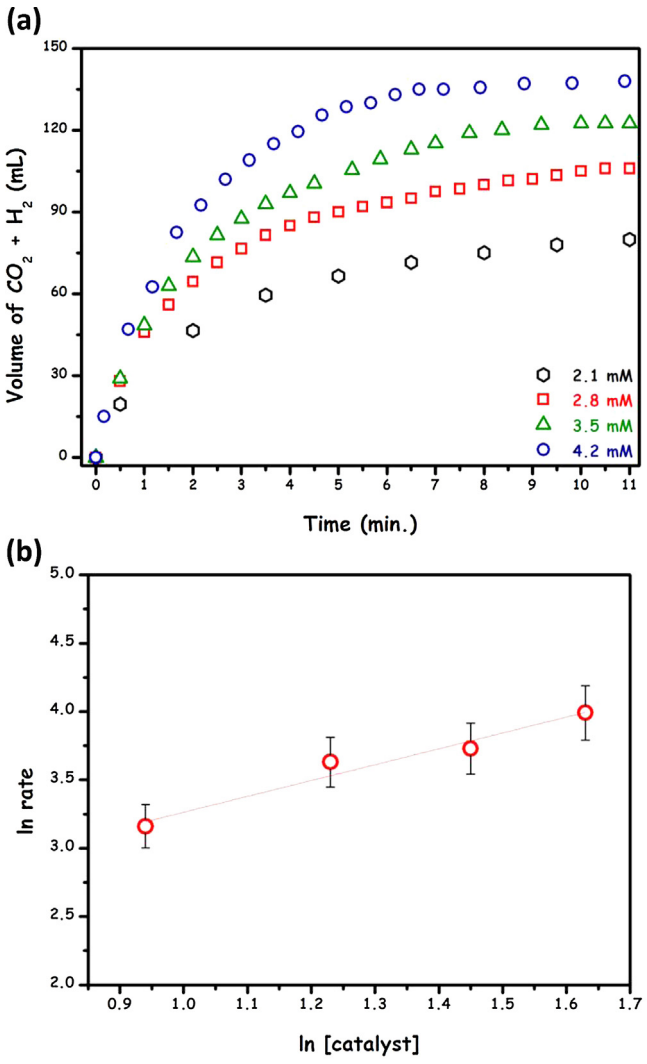

Fig. 9. (a) The volume of the generated gas ($CO_2 + H_2$) versus time graph and (b) plot of the hydrogen-generation rate versus the catalyst concentration (both in logarithmic scale; $y = (2.10 \pm 0.44) + (1.16 \pm 0.34)x$ and $R^2 = 0.98$) for the dehydrogenation of aqueous FA catalyzed by Pd-MnO_x/SiO_2-NH_2 at different catalyst concentrations ([catalyst] = [Pd] + [Mn]) and 60.0 ± 0.1 °C.

initial TOF value of 140 h^{-1} and at elevated temperatures (>20 °C), it works more effectively, which provides *initial* TOF values of 290, 710, 1300 and 2150 h^{-1} at 30, 40, 50 and 60 °C, respectively. To the best of our knowledge, TOF value obtained at 50 °C (1300 h^{-1}) is the highest value ever reported for additive-free dehydrogenation of FA (Table 1). The Arrhenius plot given in Fig. 10(b) gave us the apparent activation energy of 61.9 kJ/mol, it is still higher than that of found by Ag@Pd NPs (22 kJ/mol) [17] but lower than the majority of the previously reported catalyst systems for FA dehydrogenation [7].

3.5. Reusability performance of Pd-MnO_x/SiO_2-NH_2 catalyst in the additive-free dehydrogenation of formic acid

Isolability and reusability of Pd-MnO_x/SiO_2-NH_2 were also tested in the additive-free dehydrogenation of FA. After the complete dehydrogenation of FA, Pd-MnO_x/SiO_2-NH_2 catalyst was isolated as black powders and bottled under nitrogen atmosphere. The isolated Pd-MnO_x/SiO_2-NH_2 catalyst is redispersed in aqueous FA solution and yet an active in the dehydrogenation of FA, as given in Fig. 11(a) Pd-MnO_x NPs retain > 80% of their *initial* catalytic activity even at the fourth catalytic run. The decrease in the activity at

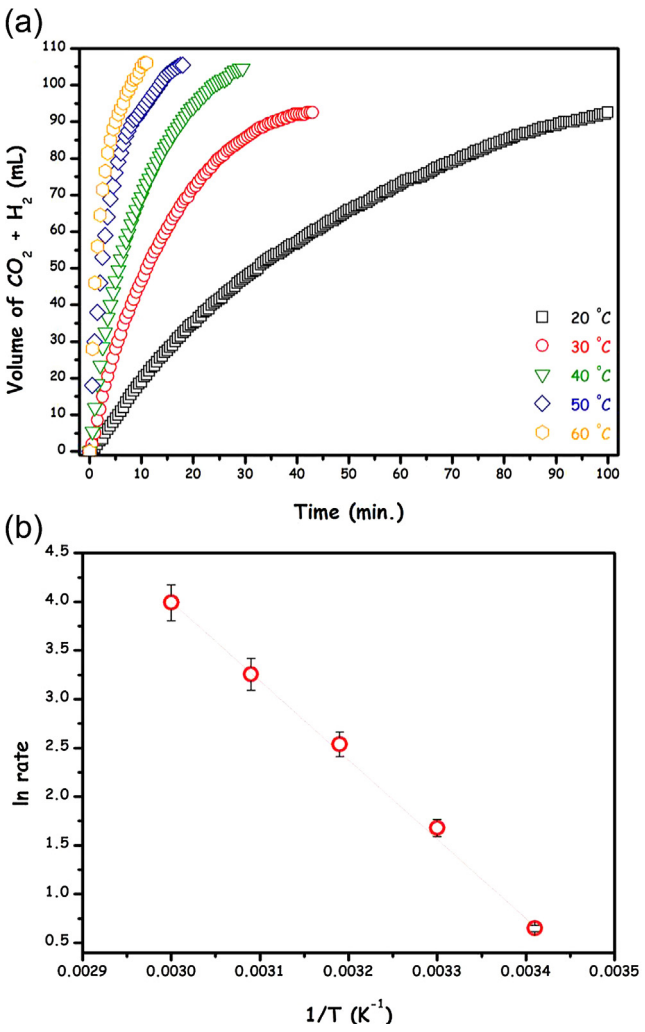

Fig. 10. (a) The volume of the generated gas ($CO_2 + H_2$) versus time at different temperatures and (b) Arrhenius plot ($y = (29.1 \pm 1.1) + (-8351 \pm 299)x$ and $R^2 = 0.99$) for the dehydrogenation of aqueous FA catalyzed by Pd-MnO_x/SiO_2-NH_2.

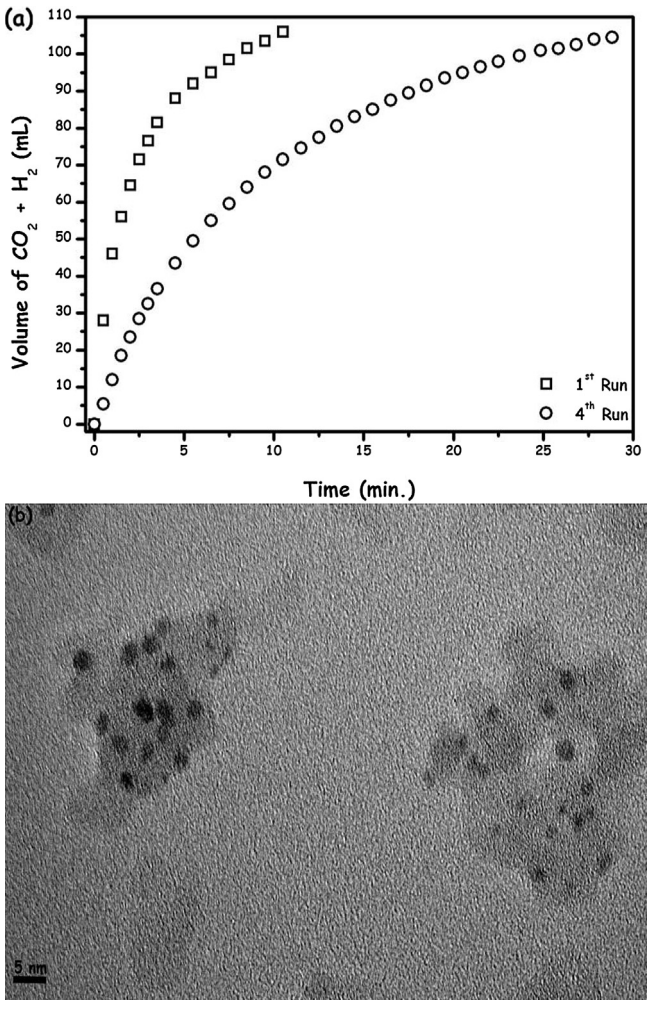

Fig. 11. (a) The volume of the generated gas ($CO_2 + H_2$) (mL) versus time (min) plot obtained from the 1st and 4th catalytic runs for the dehydrogenation of aqueous FA catalyzed by Pd-MnO_x/SiO_2-NH_2 at 60 °C, (b) representative CTEM image of Pd-MnO_x/SiO_2-NH_2 harvested after 4th catalytic run.

Table 1
Comparison of the catalytic activity for the present Pd-MnO_x/SiO_2-NH_2 catalyst with the prior best heterogeneous catalyst systems reported for the dehydrogenation FA in the absence of any additives at low temperatures.

Entry	Catalysts	T (°C)	TOF (h^{-1})	Reference
1	AuPd NPs	50	230	[16]
2	AgPd NPs	50	380	[17]
3	Au@Pd NPs	25	89	[19]
4	Ag@Pd NPs	20	125[b]	[20]
5	Ag/Pd NPs	20	144[b]	[20]
6	Ag@Pd NPs	50	252	[20]
7	CoAuPd NPs	25	80	[21]
8	Pd-MnO_x NPs	20	140	This study
9	Pd-MnO_x NPs	50	1300	This study

[a] Apart from entries 4 and 5, the TOF values given in this table are not corrected for the number of exposed surface atoms; that is, the values given are lower limits.
[b] The TOF values given in the entries 4 and 5 were determined by considering only the number of active Pd sites (upper limits).

4th reuse of $PdMnO_x/SiO_2$-NH_2 can be attributed to a decrease in the number of active surface atoms due to a small increase in the size of Pd-MnO_x NPs from 2.6 ± 0.9 to 5.4 ± 1.1 nm (Fig. 11(b)). ICP-OES analyses of the same sample gave us almost the identical Pd and Mn loading amounts with that of the fresh catalyst. Additionally, FA dehydrogenation was completely stopped by the removal of Pd-MnO_x/SiO_2-NH_2 from the reaction solution; these results confirm the retention of active Pd-MnO_x on the support and no leaching of active catalyst to the solution.

4. Conclusions

In summary, our study of the preparation and characterization of Pd-MnO_x/SiO_2-NH_2 catalyst for the dehydrogenation of formic acid has led to the following conclusions and insights:

(a) Pd-MnO_x/SiO_2-NH_2 can easily and reproducibly be prepared, for the first time, at room temperature by wet-impregnation of Pd^{2+} and Mn^{2+} onto support followed by their reduction with $NaBH_4$ in aqueous solution all at room temperature. The characterization of Pd-MnO_x/SiO_2-NH_2 catalyst was done by using ICP-OES, PXRD, XPS, CTEM, HRTEM, STEM, STEM-EDX and HAADF-STEM analyses. The results of these multipronged analyses reveal the formation of well-dispersed (4.6 ± 1.2 nm) bimetallic Pd-MnO_x NPs on SiO_2-NH_2 support throughout the separate nucleation of Pd(0) and MnO_x.
(b) The dispersion of Pd-MnO_x/SiO_2-NH_2 in the aqueous FA solution acts as a superb catalyst in terms of activity and selectivity in the additive-free dehydrogenation of FA under mild conditions. CO-stripping voltammetry analyses performed on Pd-MnO_x/SiO_2-NH_2 and Pd/SiO_2-NH_2 showed that the

existence of separately nucleated MnO_x NPs enhances CO-poisoning resistivity of active Pd NPs.

(c) The resulting Pd-MnO_x/SiO_2-NH_2 catalyst provides unprecedented activity (TOF = 1300 h^{-1} at 50 °C) at high conversion (>99%) and selectivity (>99%) among the previously reported best heterogeneous catalysts tested in the additive-free dehydrogenation of FA under mild conditions (<90 °C).

(d) The complete dehydrogenation of FA is achieved even in successive runs performed by redispersing Pd-MnO_x/SiO_2-NH_2 isolated from the previous run. When reused, Pd-MnO_x/SiO_2-NH_2 catalyst retains >80% of its initial activity even for the fourth run with a complete conversion of FA to H_2 and CO_2. Thus, Pd-MnO_x/SiO_2-NH_2 is an isolable, bottleable and reusable catalyst in the additive-free dehydrogenation of FA. Moreover, ICP-OES, P-XRD and CTEM analyses of the sample harvested from the fourth catalytic run showed that Pd-MnO_x/SiO_2-NH_2 show exceptional stability against to clumping and leaching throughout the catalytic runs in the additive-free dehydrogenation of FA.

Acknowledgments

M.Z. thanks to Yüzüncü Yıl University (BAP-2013-FEN-B015) for the financial support to his research laboratory. Additionally, the partial supports by Fevzi Akkaya Scientific Activities Support Fund (FABED), Science Academy and Turkish Academy of Sciences (TUBA) are gratefully acknowledged.

Appendix A. Supplementary data

Supplementary data associated with this article can be found, in the online version, at http://dx.doi.org/10.1016/j.apcatb.2014.09.041.

References

[1] J. Graetz, Chem. Soc. Rev. 38 (2009) 73–82.
[2] N.Z. Muradova, T.N. Veziroglu, Int. J. Hydrogen Energy 30 (2005) 225–237.
[3] J.A. Turner, Science 285 (1999) 687–689.
[4] L. Schlaphach, A. Zuttel, Nature 414 (2001) 353–358.
[5] J. Wang, X.-B. Zhang, Z.-L. Wang, L.M. Wang, Y. Zhang, Energy Environ. Sci. 5 (2012) 6885–6888.
[6] J. Wang, Y.-L. Qin, X. Liu, X.-B. Zhang, J. Mater. Chem. 22 (2012) 12468–12470.
[7] S. Enthaler, J.V. Langermann, T. Schmidt, Energy Environ. Sci. 3 (2010) 1207–1217.
[8] M. Yadav, Q. Xu, Energy Environ. Sci. 5 (2012) 9698–9725.
[9] K.V. Kordesch, G.R. Simader, Chem. Rev. 95 (1995) 191–207.
[10] T.C. Johnson, D.J. Morris, M. Wills, Chem. Soc. Rev. 39 (2010) 81–88.
[11] M. Zahmakiran, S. Özkar, Nanoscale 3 (2011) 3462–3481.
[12] M. Ojeda, E. Iglesia, Angew. Chem. Int. Ed. 48 (2009) 4800–4803.
[13] Q.Y. Bi, X.L. Du, Y.M. Liu, Y. Cao, H.Y. He, K.N. Fan, J. Am. Chem. Soc. 134 (2012) 8926–8933.
[14] X. Gu, Z-H. Lu, H-L. Jiang, T. Akita, Q. Xu, J. Am. Chem. Soc. 133 (2011) 11822–11825.
[15] Q.L. Zhu, N. Tsumori, Q. Xu, Chem. Sci. 5 (2014) 195–199.
[16] Ö. Metin, X. Sun, S. Sun, Nanoscale 5 (2013) 910–912.
[17] S. Zhang, Ö. Metin, Su D D., S. Sun, Angew. Chem. Int. Ed. 52 (2013) 3681–3684.
[18] Y.L. Qin, J. Wang, F.Z. Meng, L.M. Wang, X.B. Zhang, Chem. Commun. 49 (2013) 10028–10030.
[19] Z.L. Wang, J.M. Yan, H.L. Wang, Y. Ping, Q. Jiang, J. Mater. Chem. A 1 (2013) 12721–12725.
[20] K. Tedsree, T. Li, S. Jones, C.W.A. Chan, K.M.K. Yu, P.A.J. Bagot, E.A. Marquis, G.D.W. Smith, S.C.E. Tsang, Nat. Nanotech. 6 (2011) 302–307.
[21] Z.L. Wang, J.M. Yan, Y. Ping, H.L. Wang, W.T. Zheng, Q. Jiang, Angew. Chem. Int. Ed. 52 (2013) 4406–4409.
[22] K. Mori, M. Dojo, H. Yamashita, ACS Catal. 3 (2013) 1114–1119.
[23] I. Taylor, A.G. Howard, Anal. Chim. Acta 271 (1993) 77–85.
[24] Y. Zhang, J. Ouyang, H. Yang, Sci. Rep. 3 (2013) 1–6.
[25] M. Kang, E.D. Park, J.M. Kim, J.E. Yie, Appl. Catal. A 327 (2007) 261–269.
[26] X. Wang, Q. Kang, D. Li, Appl. Catal. B 86 (2009) 166–175.
[27] J.F. Bondi, K.D. Oyler, X. Ke, P. Schiffer, R.E. Schaak, J. Am. Chem. Soc. 131 (2009) 9144–9145.
[28] P.Z. Si, E. Brueck, Z.D. Zhang, O. Tegus, W.S. Zhang, K.H.J. Buschow, J.C.P. Klaasse, Mater. Res. Bull. 40 (2005) 29–37.
[29] J.E. Hutchison, G.H. Woehrie, S. Özkar, R.G. Finke, Turkish J. Chem. 30 (2006) 1–6.
[30] Y. Li, M. Afzaal, P. O'Brien, J. Mater. Chem. 16 (2006) 2175–2180.
[31] L. Liu, H. Liang, H. Yang, J. Wei, Y. Yang, Nanotechniques 22 (2011) 015603–015611.
[32] V. Mazumder, M. Chi, K.L. More, S. Sun, Angew. Chem. Int. Ed. 49 (2010) 9368–9371.
[33] V. Mazumder, M. Chi, K.L. More, S. Sun, J. Am. Chem. Soc. 132 (2010) 7848–7849.
[34] S. Guo, S. Zhang, D. Su, S. Sun, J. Am. Chem. Soc. 135 (2013) 13879–13884.
[35] M. Yadav, A.K. Singh, N. Tsumori, Q. Xu, J. Mater. Chem. 22 (2012) 19146–19150.
[36] M. El-Deab, A.L. Kiebler, D.M. Kolb, Electrochem. Commun. 11 (2009) 776–778.
[37] M. Yadav, T. Akita, N. Tsumori, Q. Xu, J. Mater. Chem. 22 (2012) 12582–12586.
[38] M. Zahmakiran, M. Tristany, K. Philippot, S. Özkar, B. Chaudret, Dalton Trans. 41 (2012) 590–598.
[39] M. Zahmakiran, M. Tristany, K. Philippot, K. Fajerwerg, S. Özkar, B. Chaudret, Chem. Commun. 46 (2010) 2938–2940.